



ELSEVIER

Surface Science 375 (1997) 293–301

surface science

Transmission electron diffraction determination of the Ge(001)-(2 × 1) surface structure

C. Collazo-Davila *, D. Grozea, E. Landree, L.D. Marks

Department of Materials Science and Engineering, Northwestern University, Evanston, IL 60208, USA

Received 1 August 1996; accepted for publication 28 October 1996

Abstract

The lateral displacements in the Ge(001)-(2 × 1) surface reconstruction have been determined using transmission electron diffraction (TED). The best-fit model includes displacements extending six layers into the bulk. The atomic positions found agree with X-ray studies to within a few hundredths of an ångström. With the positions determined so precisely, it is suggested that the Ge(001)-(2 × 1) surface can now serve as a standard for comparison with theoretical surface structure calculations. The results from the currently available theoretical studies on the surface are compared with the experimentally determined structure. © 1997 Elsevier Science B.V. All rights reserved.

Keywords: Computer simulations; Electron energy loss spectroscopy; Ge(001)-(2 × 1); Germanium; Low index single crystal surfaces; Surface relaxation and reconstruction; Transmission high-energy electron diffraction

1. Introduction

The (2 × 1) reconstruction on Si(001) and Ge(001) has been the focus of many investigations since it was first observed [1] using low energy electron diffraction (LEED) in 1959. Today many details about the structure and dynamics of the two surfaces are known. It is generally accepted that the basic building block of the Si(001) and Ge(001) reconstructions is an asymmetric dimer (see Fig. 1). Atoms on the (001) surface satisfy dangling bonds by bonding with neighbors along a <110> direction. The dimer atoms, however, do not move toward each other equal amounts. One atom is pulled slightly into the surface while the other is pushed out forming a tilted dimer with

two possible orientations. The dimers line up in parallel rows and by an ordering of their tilt directions can form higher order reconstructions. Several room temperature diffraction experiments [2–8] have reported diffuse streaks at p(2 × 2) and c(4 × 2) locations indicating that some ordering of the dimer tilts is present along dimer rows. Sharp superstructure spots have only been seen upon cooling down to ~200 K for Ge(001) [4,5,7,8]. Theoretical total energy minimization calculations [9–13] show either the p(2 × 2) or c(4 × 2) structure to have the lowest energy, but the experimental investigations indicate that the c(4 × 2) structure is favored on both Si and Ge.

While early total energy minimization calculations and experimental studies supported the tilted dimer model, the first scanning tunneling microscopy (STM) study on Si(001) [14] sparked some debate by showing mostly symmetric dimers

* Corresponding author. Fax: +1 847 491 7820.

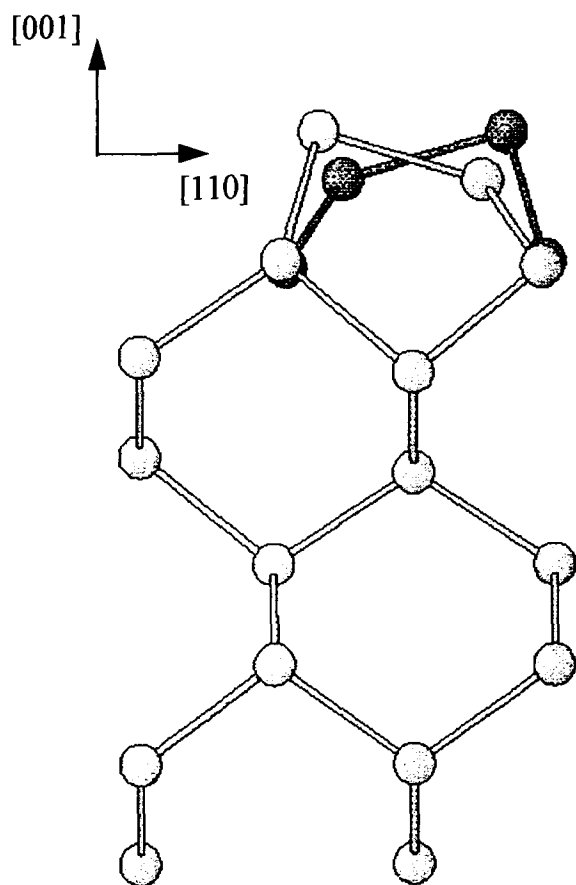


Fig. 1. A side view of the best fit model. The top two layers have been split into the two possible dimer orientations with a one-half occupancy for each atom. This simulates a random array of asymmetric dimers.

on the surface. The few dimers that appeared tilted were localized near surface defects. The authors of the STM paper suggested that at room temperature the dimers were flipping orientation rapidly in comparison to the scanning rate, so that the STM images provided a time-averaged representation of an asymmetric dimer. Using the calculated energy difference between a symmetric dimer and a tilted dimer as the energy barrier to be surmounted in a flip, Dabrowski and Scheffler [15] estimated the flipping rate would be 10^9 s^{-1} for Si, and Kruger and Pollmann [16] estimated that for Ge it would be 10^3 times smaller than for Si.

The first detailed experimental structural study on the Ge(001)-(2 × 1) surface [17] was not

attempted until 1992. This grazing incidence X-ray diffraction experiment reported atomic positions up to 10 layers down from the surface. Since then two more X-ray studies have been reported – one on Ge(001)-(2 × 1) [18] and one on Ge(001)-c(4 × 2) at 150 K [19]. In this paper we describe a TED study of the room temperature Ge(001)-(2 × 1) structure. The in-plane atomic positions we find agree with all three X-ray studies to within a few hundredths of an ångström. Such a precise experimental consensus allows the Ge(001) surface to serve as a valuable model system for theoretical studies of native surface reconstructions.

2. Experimental procedure

3 mm discs were cut from a (001) oriented germanium wafer and mechanically thinned to 200 μm . The discs were then dimpled to 30 μm thickness in the center and chemically etched (HNO_3 :HF 9:1) until a small hole appeared. The regions around the edge of the hole in such a sample are on the order of hundreds of ångströms thick and are suitable for transmission electron microscopy (TEM) observation.

After thinning, the sample was placed inside the SPEAR surface science analysis system [20]. The SPEAR system is equipped with X-ray photoelectron spectroscopy (XPS), Auger electron spectroscopy (AES), scanning electron microscopy (SEM) and ion milling capabilities, and it is attached to a high resolution UHV H-9000 Hitachi transmission electron microscope. The base pressure in the surface analysis region of SPEAR is $\sim 5 \times 10^{-11}$ Torr, and the operating pressure in the objective lens region of the microscope where the sample sits is $\sim 8 \times 10^{-11}$ Torr with the electron beam on. Inside SPEAR, an oxygen ion mill (4 kV, 60° from surface normal) followed by an argon ion mill (3 kV, 60° from surface normal) and an anneal at 400°C for 4 min removed most of the surface contamination from the sample. The chemical purity of the germanium surface was monitored with XPS, and since TEM probes both the top and bottom surfaces, both sides of the sample were cleaned.

The microscope was used to investigate the

development of the surface structure between milling/annealing cycles. After the first cycle, a faint 2×1 periodicity appeared in the TED pattern. Further cycles of argon ion milling and annealing at 500°C were used to strengthen the 2×1 pattern and then the diffracted beam intensities were recorded using both film and a parallel electron energy loss spectroscopy (PEELS) unit mounted in the microscope. Before the data were collected, the germanium crystal was tilted off the (001) zone in order to attenuate the bulk reflection intensities relative to the surface reflection intensities [21]. For the film data, a series of nine negatives were exposed with increasing exposure times from 0.5 to 120 s. For the PEELS data, the transmitted beam and eight of the strongest diffracted beams were deflected into the unit, and spectra from zero energy loss to 500 eV loss were recorded digitally. By measuring the bulk spot intensities relative to the transmitted beam with PEELS, we could make absolute comparisons between simulated and measured diffraction intensities during the fitting process.

3. Data analysis

The nine diffraction pattern negatives were digitized to eight bits with a $25 \mu\text{m}$ pixel size using an Optronics P-1000 microdensitometer. Fig. 2 shows the central region of a composite of two digitized diffraction patterns. Reflections from both 2×1 and 1×2 domains are present. The diffraction spots can be separated into three categories: bulk reflections which arise from the bulk diamond cubic germanium lattice, 1×1 reflections having the periodicity of the unreconstructed (001) surface, and pure surface reconstruction reflections which arise from the 2×1 or 1×2 surface unit cells. The 1×1 spots have intensity contributions from both the surface step structure as well as the surface reconstruction and so were not considered in our analysis. The splitting of the 1×1 spots seen in Fig. 2 indicates a periodic array of steps on the surface with an average spacing of $\sim 70 \text{ \AA}$. Measurements of the bulk spots were used to help determine both the incident electron beam tilt with respect to the crystal axes and the sample thickness.

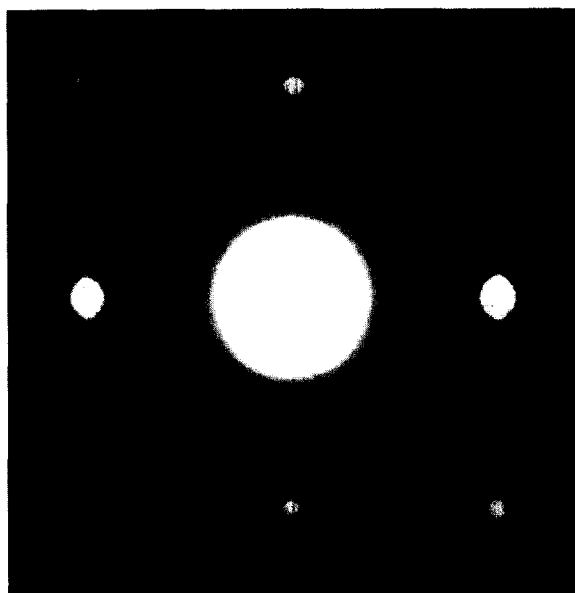


Fig. 2. Composite of two different exposure time Ge(001)-(2×1) diffraction patterns. The arrowed surface spot is shown in the inset at the top left magnified eight times to show the anisotropic shape due to domain size. Periodic steps on the surface cause the splitting seen in the 1×1 spots.

While the bulk spots appear round, the surface reconstruction spots are elongated indicating anisotropic surface domain sizes. Since both 2×1 and 1×2 domains must terminate at surface steps and all of the surface spots are elongated along the same direction, the anisotropy can be attributed to surface steps running along the direction perpendicular to the elongation of the spots. Relative beam intensities were measured using a cross-correlation technique developed by our group [22]. For each negative, eight strong but non-saturated spots were chosen, independently scaled to unit integrated intensity, and then averaged together to form a motif representing the general shape of a diffraction spot. Separate motifs were formed for bulk and surface reflections since their shapes differed. After the formation of the two motifs, a software routine scanned through the negative comparing each non-saturated spot with the appropriate motif. For the comparison, the center of the spot to be measured was found by cross-correlation with the motif. With the centers of the spot and the motif precisely aligned, a least

squares fit was calculated over a 32×32 pixel region assuming that the measured spot was simply a scaled up version of the motif. In this manner, the intensities of all the surface spots on a given negative were determined relative to each other. In the PEELS data, a one-dimensional analog of the cross-correlation method was used to obtain the relative intensities of the transmitted beam and strong bulk spots, and in the following analysis the PEELS intensity data were treated the same as if coming from a tenth negative with its own exposure time.

Next, to compare intensities from different negatives in the exposure series, scaling factors between the pictures were defined. Denoting the scaling factor between pictures 1 and 2 as s_1 , the scaling between 2 and 3 as s_2 , and so on, there were a total of 9 factors ending with s_9 . These factors were calculated by minimizing the quantity,

$$\sum_{i=1,9} \sum_{j=(i+1),10} \sum_n (I_{i,n} - S_{i,j} I_{j,n})^2, \quad (1)$$

where $S_{i,j} = (s_i)(s_{i+1}) \dots (s_{j-1})$ represents the scaling between pictures i and j , and $I_{i,n}$ is the intensity of beam number n in picture i . The sum over n is taken over all beams which were measured in both pictures i and j . Many beams were measured on as many as six negatives in the middle of the exposure time series. Using the multiple measurements and the calculated scaling factors, average intensities scaled to the shortest exposure time were found. Since we used dynamical diffraction calculations to refine the model structure, we did not average over kinematically symmetry equivalent spots, and a total of 372 surface intensities appeared in the final data set.

Due to the digitization process, there is a fixed window of optical density which we can measure on a negative regardless of exposure time. However, as the exposure time increases, the background noise on the film increases relative to the fixed measurement window. To account for this increasing uncertainty in intensity measurements, we calculated a separate variance for the data from each negative. The variances were then used for error estimates of individual measurements when calculating a final average value and associated error.

While most intensities were measured using cross correlation as described above, a sizeable number of the diffraction spots (about 30%) were on top of a diffuse background which caused the cross correlation routine to overestimate their intensity. In these cases the intensity measurement was taken visually by subtracting off scaled versions of the motif until only a noisy background was left. Along with the intensity measurement, upper and lower bounds of certainty were also recorded for each spot to provide an estimate of the measurement error. Examination of the error estimates for all the visually measured spots showed the absolute magnitude of the error to be roughly constant, and this constant error was added in quadrature to the variance calculated as mentioned before.

4. Fitting procedure

While kinematical diffraction theory provides a good description of weakly scattering X-rays, a dynamical approach is needed for the more strongly scattered electrons used in our experiment. Diffraction intensities were simulated with the Northwestern University Multislice and Imaging System (NUMIS) package. In the standard multislice approach used by NUMIS, the crystal is cut into slices perpendicular to the direction of the incident electron plane wave. The scattering calculations are performed slice by slice as the wave propagates through the crystal. In the case of germanium each bulk unit cell was cut four times so that a single slice was 1.4 \AA thick. Since our data is insensitive to displacements parallel to the incident electron beam, and the incident electron beam was nearly perpendicular to the Ge(001) surface, we only considered displacements parallel to the surface. All of the models tested consisted of either one or two reconstructed unit cells (four or eight slices) on both the top and bottom surfaces separated by bulk material. As mentioned in the introduction, the estimated dimer flipping rate at room temperature is on the order of 10^6 s^{-1} for the Ge(001) surface. In comparison, the electron interaction time in a high resolution TEM is on the order of picoseconds. Therefore our diffraction data are insensitive to the flipping

dynamics of the dimers, and we did not have to take into account any time-averaging effects.

The measured bulk spots were used to estimate the sample thickness and the incident beam tilt with respect to the (001) zone axis. Initially a visual comparison with simulated diffraction patterns found the tilt to within a few milliradians and narrowed the possible thickness down to three ranges near 100, 300 and 600 Å. By analyzing the structure in convergent beam electron diffraction (CBED) patterns one can measure crystal thickness very precisely [23]. However, the region from which the 2×1 diffraction data was taken was too thin to apply the CBED technique. As an alternative, the PEELS spectrum of the transmitted beam was analyzed using the relation, $t/\lambda = \ln(I_t/I_0)$, where t is the thickness, λ is the inelastic mean free path, I_t is the total number of electrons in the spectrum and I_0 is the number of electrons in the zero loss peak [24]. λ for the Ge sample was measured by gathering CBED and PEELS data from thicker regions to define the relationship between t and $\ln(I_t/I_0)$. A linear relationship was verified and extrapolated down to lower values of t where the PEELS spectra indicated a thickness near 100 Å. Finally, a numerical R -factor minimization refined the values for the thickness and tilt to 76 Å and 100 mrad respectively. An overall scaling term included in the R -factor fit was 2.5, indicating a reasonable agreement between the absolute magnitudes of the measured and simulated intensities.

In all the models considered, both 2×1 domains and 1×2 domains were assumed to exist on the top and bottom surfaces, requiring four separate multislice calculations for each iteration of the minimization program. The four calculations were averaged together to form the final simulated diffraction intensities. The relative weightings of the four calculations in the final average were included as four additional fitting parameters. In agreement with Rossmann et al. [17] and Torrelles et al. [18] the best fit model for our data was a disordered array of buckled dimers shown in Fig. 1. The random disorder in the buckling direction was simulated by including both possible dimer orientations in a unit cell with a 1/2 fractional occupancy. The fractional occupancy was simulated in only the first two layers of atoms. Isotropic

Debye–Waller factors for the first two layers were also included in the fit, and the factors for all other layers were fixed at the bulk value.

A reduced χ^2 value defined as,

$$\chi^2 = \frac{1}{N - M} \sum_{j=1}^N \left(\frac{I_{\text{meas}}^j - I_{\text{calc}}^j}{\sigma_j} \right)^2, \quad (2)$$

was initially used as a measure of the goodness of fit, where N is the total number of measured intensities, M is the number of parameters allowed to vary in the fit, $I_{\text{meas}/\text{calc}}$ is a measured/calculated beam intensity and σ_j is the error for the j th intensity. The value of χ^2 provides a measure of the probability of making a given set of observations [25]. Assuming that a particular model is correct so that all simulated values are accurate and that the measurement errors associated with collecting the data have Gaussian distributions of known widths (the σ_j 's), the probability of taking a data set that would produce a χ^2 value much different from 1 decreases rapidly with increasing number of data points. For our best fit model we found a χ^2 value of 2.36. With 372 data points in our fit, the probability is infinitesimally small that we would obtain a χ^2 value of 2.36 assuming the model is correct and all of the error estimates are accurate.

A key assumption in a χ^2 analysis is that the errors between the measurements and the simulation have Gaussian distributions. Fig. 3 is a plot

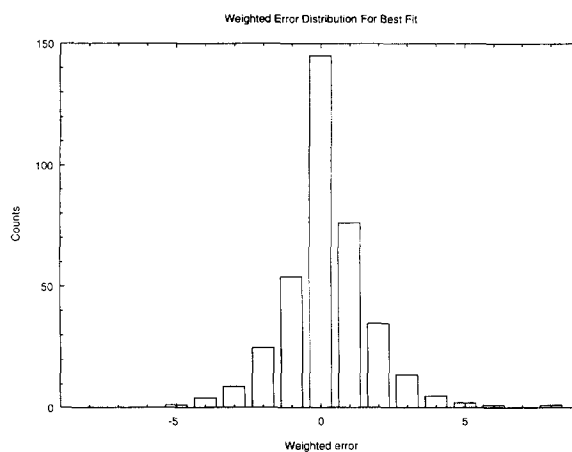


Fig. 3. Distribution of weighted errors in the best χ^2 fit for all 372 measured beams.

of the distribution of errors for our χ^2 fit. Instead of being Gaussian, the distribution is much closer to an exponential distribution of the form $\exp(-|x|)$, so the use of a χ^2 analysis cannot be justified in this case. The reason for the exponential distribution lies in the method of simulation. In looking at the fit beam by beam, we noticed that the worst fit beams all appeared adjacent to the zeroth order Laue zone in the diffraction pattern and were all much stronger than in the simulation. This suggests that the reconstruction is not limited to a two-dimensional surface layer but rather extends into the bulk. To properly simulate such three-dimensional effects, we would have to make the slices used in the multislice extremely thin, which would translate into prohibitively long calculation times. By necessity we used the 1.4 Å thick slices and found the exponential distribution of fitting errors. A robust χ analysis [26] is analogous to a χ^2 analysis with the assumption of Gaussian errors replaced by an assumption of exponentially distributed errors, and therefore is more appropriate for our case. The χ parameter is defined as,

$$\chi = \frac{1}{N - M} \sum_{j=1}^N \left(\frac{|I_{\text{meas}}^j - I_{\text{calc}}^j|}{\sigma_j} \right). \quad (3)$$

The χ factor is similar to χ^2 and for a reasonable fit will tend toward a value of 1, but it is less sensitive to points with large errors. While in the calculation of χ^2 a large value of $I_{\text{meas}} - I_{\text{calc}}$ for a poorly fit beam will be squared and will contribute significantly to the sum, the same $I_{\text{meas}} - I_{\text{calc}}$ in the calculation of χ will only be a few times larger than most of the other 372 terms in the sum and will not be treated with undue importance.

5. Results

The atom positions for our best fit model are shown in Table 1 along with the results of three X-ray studies. The Debye–Waller factors for layers one and two were 3.9 times and 2.5 times the bulk value, respectively. While both χ^2 and χ factors were calculated, we show only the results for the χ minimization as explained above. In any case,

the atom positions only differed by at most a couple of hundredths of an ångström between the two treatments. The χ value for the fit shown is 1.10. Although the magnitudes of the atom displacements in the 5th and 6th layers are only 0.05 and 0.04 Å, respectively, they had a significant effect on the goodness of fit. For a model with only the first two layers allowed to move, the lowest χ value obtained was 1.63. Including the 5th and 6th layer displacements in the model dropped the χ value down to 1.10. For comparison, the χ^2 value in the same case fell from 5.64 to 2.36. Other models for the reconstruction were tested including a symmetric dimer and an ordered array of tilted dimers, but none provided an adequate fit.

6. Discussion

Overall the agreement between the experimental studies is excellent. If one averages the values found in the four studies for each atom position, one finds that for almost every position the largest deviation from the average occurs in the study by Rossmann et al. [17]. This can be attributed to the relatively smaller data set size measured in that study. The positions for the first dimerized layer are all within 0.07 Å of each other, and even though the individual second layer positions show some more scatter (0.24 Å) the distances between the two second layer atoms all agree to within 0.08 Å. It is not surprising that the relative separation of atoms in a given layer are determined more accurately than the individual atom positions, since the thermal vibrations of neighboring atoms are likely to be correlated. While the vibration amplitude for a given atom could be relatively large near the surface, its vibrational amplitude relative to its neighbor would be significantly less.

It is interesting to note the close agreement for the dimer structure between the room temperature (2×1) studies and the 150 K $c(4 \times 2)$ study. Northrup [17] reported a similar agreement between room temperature photoemission measurements and the surface band structure calculated for the Si(001)- $c(4 \times 2)$ reconstruction. He pointed out that the agreement suggests a strong correlation of dimer tilt directions along a dimer row. In fact,

Table 1

Comparison of experimental results from this study: X-ray studies of the 2×1 structure and an X-ray study of the $c(4 \times 2)$ structure

| Current study 372 in-plane | Rossmann et al. [17] 42 in-plane averaged to 13, 71 out-of plane | Torrelles et al. [18] 126 in-plane averaged to 48, 428 out-of-plane averaged to 242 | | Ferrer et al. $c(4 \times 2)$ [19] 46 in-plane, 165 out-of-plane (no 2×1 beams included) | |
|-------------------------------|--|--|-------|---|--------------------|
| X | X | X | Y^c | X | Y |
| 0.123 | 0.129 | 0.120 | 0.0* | 0.1210 | 0.0* |
| 0.421 | 0.422 | 0.427 | 0.0* | 0.4216 | 0.0* |
| 0.017 | -0.007 | 0.001 | 0.5* | 0.0164 ^a | 0.529 ^b |
| 0.490 | 0.458 | 0.476 | 0.5* | 0.4836 ^a | 0.471 ^b |
| 0.25* | 0.25* | 0.25* | 0.5* | 0.25* | 0.5* |
| 0.75* | 0.75* | 0.75* | 0.5* | 0.75* | 0.5036 |
| 0.25* | 0.25* | 0.25* | 0.0* | 0.2526 | 0.0* |
| 0.75* | 0.75* | 0.75* | 0.0* | 0.75* | 0.0* |
| -0.0061 ^a | -0.009 ^a | -0.0047 ^a | 0.0* | - | - |
| 0.5061 ^a | 0.509 ^a | 0.5047 ^a | 0.0* | - | - |
| -0.0052 ^b | -0.004 ^b | -0.0021 ^b | 0.5* | - | - |
| 0.5052 ^b | 0.504 ^b | 0.5021 ^b | 0.5* | - | - |

The size of the data set in each study is indicated at the top of each column, with averaging over kinematically symmetry-equivalent reflections. As explained in the text no symmetry averaging was done in the current study, and all of the reflections measured in the study by Ferrer et al. were non-symmetry related. Numbers are in terms of the (2×1) unit cell with $X_0 = 8 \text{ \AA}$ and $Y_0 = 4 \text{ \AA}$. The atom positions from the $c(4 \times 2)$ study of Ferrer et al. have been reduced relative to this same (2×1) notation so direct comparisons can be made.

* Denotes a parameter that is fixed.

^{a,b} Denotes two parameters that are symmetry related.

^c This column of Y positions is common to the first three columns of X positions.

many studies have provided evidence for correlated buckling of dimers at room temperature. Several studies have shown that in the formation of higher order reconstructions, the dimer interaction along a dimer row is much stronger than the interaction between rows [5,8,19]. In STM studies [14,28–30] some rows of alternating tilted dimers can be seen. Other diffraction studies [2–8] have shown diffuse streaks through $c(4 \times 2)$ positions indicating that some short range ordering is taking place. In our data the $c(4 \times 2)$ streaks were also seen on the longer exposure time negatives (Fig. 4). A temperature dependent X-ray study by Lucas et al. [8] indicated that the alternating tilting continues for about 80 \AA (20 unit cells) along dimer rows at room temperature. Based on temperature dependent photoelectron spectroscopy measurements, Landmark et al. [31] have argued that the room temperature $\text{Ge}(001)\text{-}2 \times 1$ and $\text{Si}(001)\text{-}2 \times 1$ surfaces should actually be viewed as disordered $c(4 \times 2)$ surfaces.

The similarity between the (2×1) dimer and the

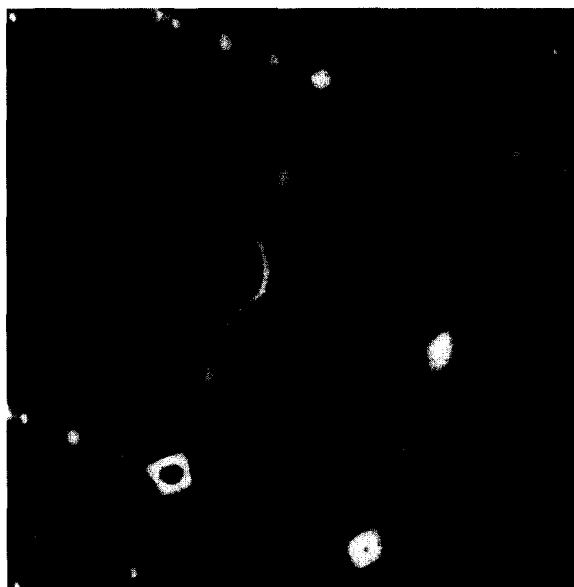


Fig. 4. $\text{Ge}(001)\text{-}(2 \times 1)$ diffraction pattern that has been high-pass filtered to highlight the $c(4 \times 2)$ diffuse streaks. Arrows indicate two streaks passing through $c(4 \times 2)$ locations.

$c(4 \times 2)$ dimer seen in Table 1 is consistent with correlated buckling along dimer rows. Since there exists a strong interaction between dimers along a dimer row, the atomic positions of the two atoms in a dimer will be affected by the tilt direction of the two neighboring dimers in the row. The agreement between the atomic positions in the (2×1) and $c(4 \times 2)$ dimers suggests that the local environment for the majority of (2×1) dimers is similar to that in $c(4 \times 2)$, i.e. dimers along a row alternate buckling direction. However, the lack of sharp $c(4 \times 2)$ or $p(2 \times 2)$ spots indicates that the correlation is only short range, and the disordered dimer model can still provide a good fit.

The results of the three theoretical studies [11,13,32] reporting atomic positions known to the authors are shown in Table 2. Both theory and experiment indicate a projected dimer bond length of 2.40 Å. All of the studies lie within 0.06 Å of this value. However, the theoretical calculations tend to overestimate the asymmetry of the dimer. Looking at the x position for the first atom in the dimer, one sees that the experimental results range from 0.96 to 1.03 Å while the theoretical results range from 1.12 to 1.21 Å. This discrepancy is possibly due to differences in modeling. In each case the experimental data were fit best by a disordered array of buckled dimers, while in the theoretical (2×1) calculations a perfectly ordered array of dimers had to be assumed with all the

dimers tilting in the same direction. Two of the theory studies [11,13] also considered the $c(4 \times 2)$ structure. With its alternating dimer tilts the $c(4 \times 2)$ offers a more accurate description of the room temperature surface than a true (2×1) structure with all the dimers tilting the same way. The $c(4 \times 2)$ results are shown in Table 3, and one can see that the values obtained by Needels et al. provide the best theoretical match to the experimentally determined structure.

In view of the experimental evidence, the lateral displacements in the Ge(001)- (2×1) structure can be regarded as known with a high degree of confidence. Four independent studies employing two distinct experimental techniques have reported atom positions for the first six layers. The positions agree to within a few hundredths of an ångström. It was shown that the best agreement between the experimentally determined structure and a theoretical calculation was for a calculation assuming a full $c(4 \times 2)$ unit cell. When taken with the extensive experimental evidence for correlated buckling at room temperature, this suggests that for theoretical structure calculations of the Ge(001)- (2×1) surface, the surface may be best modeled with a $c(4 \times 2)$ unit cell.

Acknowledgements

We would like to acknowledge the support of the National Science Foundation on grant #DMR-9214505 in funding this work.

Table 2

A comparison of theoretical results for the (2×1) structure; positions are in terms of the (2×1) unit cell as in Table 1

| Needels et al. [11] | Pollmann et al. [13] | Spiess et al. [32] | Y^a |
|---------------------|----------------------|--------------------|-------|
| X | X | X | |
| 0.1507 | 0.1404 | 0.1408 | 0.0* |
| 0.4475 | 0.4423 | 0.4408 | 0.0* |
| 0.0208 | 0.0069 | 0.0045 | 0.5* |
| 0.4971 | 0.4933 | 0.4889 | 0.5* |
| 0.2629 | 0.2451 | – | 0.5* |
| 0.7566 | 0.7551 | – | 0.5* |
| 0.25 | 0.25 | – | 0.0* |
| 0.75 | 0.75 | – | 0.0* |

* Denotes a parameter that is fixed.

^a This column of Y positions is common to all three columns of X positions.

Table 3

A comparison of theoretical studies for the $c(4 \times 2)$ structure; positions have been reduced relative to a (2×1) unit cell as in Table 1

| Needels et al. [11] | | Spiess et al. [13] | |
|---------------------|---------|--------------------|--------|
| X | Y | X | Y |
| 0.1174 | –0.0067 | 0.1381 | 0.0 |
| 0.4112 | –0.0049 | 0.4414 | 0.0 |
| 0.0087 | 0.4694 | 0.0078 | 0.5185 |
| 0.4839 | 0.5138 | 0.4922 | 0.4815 |
| 0.2467 | 0.5050 | – | – |
| 0.7490 | 0.5013 | – | – |
| 0.25 | 0.0 | – | – |
| 0.75 | 0.0 | – | – |

References

- [1] R.E. Schlier and H.E. Farnsworth, *J. Chem. Phys.* 30 (1959) 917.
- [2] J.J. Lander and J. Morrison, *J. Chem. Phys.* 37 (1962) 729.
- [3] M.J. Cardillo and G.E. Becker, *Phys. Rev. Lett.* 40 (1978) 1148.
- [4] S.D. Kevan and N.G. Stoffel, *Phys. Rev. Lett.* 53 (1984) 702.
- [5] S.D. Kevan, *Phys. Rev. B* 32 (1985) 2344.
- [6] R.J. Culberson, Y. Kuk and L.C. Feldman, *Surf. Sci.* 167 (1986) 127.
- [7] W.R. Lambert, P.L. Trevor, M.J. Cardillo, A. Sakai and D.R. Hamann, *Phys. Rev. B* 35 (1987) 8055.
- [8] C.A. Lucas, C.S. Dower, D.F. McMorrow, G.C.L. Wong, F.J. Lamelas and P.H. Fuoss, *Phys. Rev. B* 47 (1993) 10 375.
- [9] D.J. Chadi, *Phys. Rev. Lett.* 43 (1979) 43.
- [10] J. Ihm, D.H. Lee, J.D. Joannopoulos and J.J. Xiong, *Phys. Rev. Lett.* 51 (1983) 1872.
- [11] M. Needels, M.C. Payne and J.D. Joannopoulos, *Phys. Rev. Lett.* 58 (1987) 1765.
- [12] M. Needels, M.C. Payne and J.D. Joannopoulos, *Phys. Rev. B* 38 (1988) 5543.
- [13] L. Spiess, A.J. Freeman and P. Soukiassian, *Phys. Rev. B* 50 (1944) 2249.
- [14] R.J. Hammers, R.M. Tromp and J.E. Demuth, *Phys. Rev. B* 34 (1986) 5343.
- [15] J. Dabrowski and M. Scheffler, *App. Surf. Sci.* 56–58 (1992) 15.
- [16] P. Kruger and J. Pollmann, *Phys. Rev. Lett.* 74 (1995) 1155.
- [17] R. Rossmann, H.L. Meyerheim, V. Jahns, J. Wever, W. Moritz, D. Wolf, D. Dornisch and H. Schulz, *Surf. Sci.* 279 (1992) 199.
- [18] X. Torrelles, H.A. van der Vegt, V.H. Etgens, P. Fajardo, J. Alvarez and S. Ferrer, *Surf. Sci.* 364 (1996) 242.
- [19] S. Ferrer, X. Torrelles, V.H. Etgens, H.A. van der Vegt and P. Fajardo, *Phys. Rev. Lett.* 75 (1995) 1771.
- [20] C. Collazo-Davila, E. Landree, D. Grozea, G. Jayaram, R. Plass, P.C. Stair and L.D. Marks, *JMSA* 1 (1995) 267.
- [21] G. Jayaram, R. Plass and L.D. Marks, *Interface Sci.* 2 (1995) 379.
- [22] P. Xu, G. Jayaram and L.D. Marks, *Ultramicroscopy* 53 (1994) 15.
- [23] S.M. Allen and E.L. Hall, *Phil. Mag.* 46A (1982) 243.
- [24] T. Malis, S.C. Cheng and R.F. Egerton, *J. Electron Microsc. Techn.* 8 (1988) 193.
- [25] P.R. Bevington, *Data Reduction and Error Analysis for the Physical Sciences* (McGraw-Hill, New York, 1969) p. 81.
- [26] W.H. Press, B.P. Flannery, S.A. Teukolsky and W.T. Vetterling, *Numerical Recipes* (Cambridge University Press, Cambridge, 1986) p. 539.
- [27] J.E. Northrup, *Phys. Rev. B* 47 (1993) 10 032.
- [28] J.A. Kubby, J.E. Griffith, R.S. Becker and J.S. Vickers, *Phys. Rev. B* 36 (1987) 6079.
- [29] J. Wang, T.A. Arias and J.D. Joannopoulos, *Phys. Rev. B* 47 (1993) 10 497.
- [30] W.S. Yang, X.D. Wang, K. Cho, J. Kishimoto, S. Fukatsu, T. Hashizume and T. Sakurai, *Phys. Rev. B* 50 (1994) 2406.
- [31] E. Landemark, C.J. Karlsson, L.S.O. Johansson and R.I.G. Uhrberg, *Phys. Rev. B* 49 (1994) 16 523.
- [32] J. Pollmann, P. Kruger and A. Mazur, *J. Vac. Sci. Technol. B* 5 (1987) 945.